# Superstoichiometry, accelerated diffusion, and nuclear reactions in deuterium-implanted palladium

S. M. Myers, P. M. Richards, D. M. Follstaedt, and J. E. Schirber
*Sandia National Laboratories, Albuquerque, New Mexico 87185*
(Received 16 July 1990)

Deuterium (D) was introduced into Pd at atomic ratios greater than one by ion implantation at cryogenic temperatures. The rise and saturation of the D concentration at these low temperatures, together with the decay of the superstoichiometric state during annealing, were observed by detecting charged particles from the nuclear reaction $D(d,p)T$ when a deuteron beam impinged on the specimen. At implantation temperatures of 41 and 81 K, a saturation concentration ratio [D]/[Pd] of $1.6\pm0.2$ was reached, substantially above the limit of 1.0 observed in gas-phase charging. As the temperature was subsequently ramped upward, [D]/[Pd] abruptly decreased to approximately 1.0 near 120 K, reflecting a process of accelerated transport unique to the superstoichiometric state. The responsible diffusion mechanism was theoretically examined using analytical modeling and molecular-dynamics simulations, leading to a picture of correlated D hopping among octahedral and tetrahedral interstitial sites. Cold fusion was not detected in the absence of external ion bombardment, implying an upper bound on the reaction rate in the high-concentration deuteride of approximately $10^{-21}$ events/s D atom.

## I. INTRODUCTION

Ion implantation of deuterium (D) into Pd at a temperature of 35 K was previously reported to produce concentrations as high as 1.3 D atoms per metal atom.[1] This ratio substantially exceeds the limit of [H]/[Pd]=1.0 that is approached during high-pressure gas-phase charging near room temperature and above.[2] Recently, the discussion of possible D-D fusion reactions in Pd deuteride[3,4] prompted us to explore the low-temperature implanted state further, since the exceptional D density might be expected to enhance reaction probabilities. In the present paper we describe these studies and present four significant new findings. The first result is that the superstoichiometric condition disappears near 120 K as a result of anomalous rapid diffusion. Second, this accelerated transport is theoretically explained in terms of crowd-atom correlated hopping which occurs only at atomic ratios [D]/[Pd] above 1.0. Third, the observed diffusion behavior implies that low-temperature D implantation does indeed produce substantial supersaturation within the fcc Pd lattice, as opposed to the accumulation of excess D in defect traps and bubbles. Finally, energetic charged particles from D-D nuclear reactions were not detected after implantation stopped, yielding an upper bound on the cold-fusion reaction rate within the superstoichiometric PdD. (Preliminary results of the search for cold fusion were reported previously.[5])

The Pd specimens of these experiments were initially implanted with 10-keV D at a temperature of 41 or 81 K where the D is immobile, thereby charging the metal matrix to a depth of about 100 nm. The rise and saturation of the D concentration were monitored by detecting protons and tritons from the beam-induced nuclear reaction $D(d,p)T$. The temperature stability of the superstoichiometric state was then investigated by temperature ramping, during which the D concentration was determined by bombarding with 30-keV D and detecting the nuclear-reaction products. In treating the migration of the D theoretically, we employed classical two-body potentials similar to those previously used to describe Pd deuteride.[6] The crowd-atom diffusion mechanism in the superstoichiometric state was inferred from analytical calculations and confirmed by molecular-dynamics simulations. The search for cold fusion in the implanted Pd was carried out by monitoring charged-particle emission over a period of hours in the absence of further deuteron bombardment.

Experimental details of this work are given in Sec. II, and the data from saturation implantations and temperature ramps are presented and analyzed in Sec. III. Section IV then describes our theoretical analysis of the accelerated diffusion. The negative results of the search for cold fusion are reported in Sec. V, and our conclusions are summarized in Sec. VI.

## II. EXPERIMENTAL DETAIL

The Pd samples were rolled foils with specified purity 99.997% and dimensions of $10\times10\times0.25$ mm$^3$. Two such specimens were annealed for 16 h at 1273 K under an ion-pumped vacuum of $10^{-5}$ Pa, while a third was used in the as-rolled condition after being chemically cleaned. During ion implantation of D, the specimen was held against a Cu block by a spring-loaded stainless-steel cover plate and exposed to the beam through a circular 10-mm hole in the plate. Deuterons with an energy of 10 keV were obtained by accelerating $D_3^+$ through a potential drop of 30 kV. The implantation beam was magnetically separated to exclude $D^+$, $D_2^+$, and impurity species and was swept for uniformity. The time-averaged flux was about 4 D atoms nm$^{-2}$s$^{-1}$. The Cu block was cooled by continuous transfer of liquid He, which produced a temperature of 41 K, or by flowing liquid $N_2$,

 

which yielded 81 K; these temperatures were measured with a Cu-Constantan thermocouple on the Cu block. The implantation chamber was turbo-molecular pumped and liquid-nitrogen trapped to a base pressure of $2\times10^{-5}$ Pa.

High-energy charged particles were counted and energy-analyzed using a Si surface-barrier detector of 300-$\mu$m depletion depth which subtended a geometrically estimated solid angle of 0.20 sr at a scattering angle of 45°; this solid angle has a relatively large uncertainty of $\pm0.05$ sr, mainly due to the small detector-sample distance and the variation of this distance over the surface of the sample. The detector aperture was covered by a Ni foil of thickness 2.5 $\mu$m which ranged out the elastically backscattered D and sputtered atoms but passed 3-MeV protons and 1-MeV tritons from the reaction D($d$,$p$)T. The detection system was configured to observe particle energies up to 12 MeV after foil ranging.

Figure 1 shows part of a particle-energy spectrum obtained during ion implantation of 10 keV D. These particular data were accumulated during a 2-min interval near the end of a saturation implantation carried out at 41 K. The labeled proton and triton peaks result from nuclear reactions between energetic impinging deuterons and D already at rest within the lattice. The specific identification of these peaks is based on their energies. In the case of the protons, the initial energy of 3.02 MeV is expected to be reduced by approximately 0.16 MeV while traversing the Ni foil, resulting in a detected energy of 2.86 MeV; this is in excellent agreement with the data, which shows a peak centered at 2.90 MeV. The energy of the tritons after ranging is predicted to be $1.01-0.53$ MeV$=0.48$ MeV, in fair agreement with the peak observed at 0.57 MeV.

Background yield in the particle detection system was examined by accumulating over a period of 15 h with no Pd sample in the chamber and no impinging ion beam, and the resulting spectrum is shown in Fig. 2. Here each plotted point reflects the combined counts within eight contiguous 24-keV energy channels. The background is

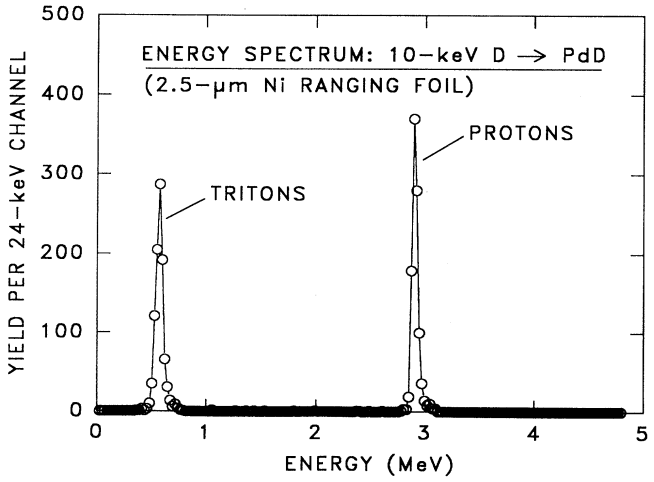


FIG. 1. Energy spectrum of charged particles from the nuclear reaction D($d$,$p$)T during ion implantation of 10-keV D into Pd. The flux was 3.6 D atoms $nm^{-2}s^{-1}$, the counting time 2 min, and the retained concentration close to saturation.

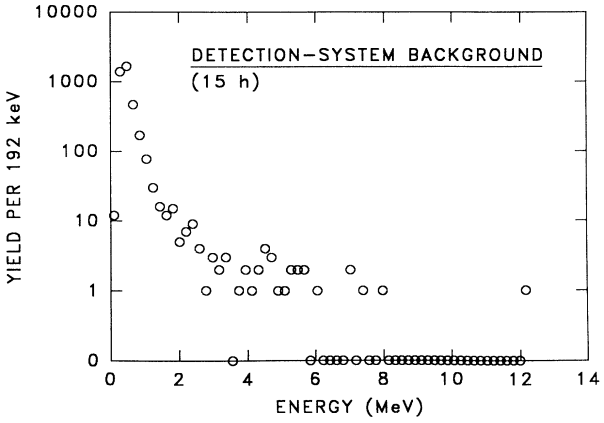


FIG. 2. Background spectrum from the particle-detection system in the absence of the Pd specimen and with no deuteron beam incident into the chamber. The accumulation time was 15 h.

seen to increase with decreasing energy, as is commonly observed in such detection systems, and it is ascribed to detector noise. The level is quite small above about 1.5 MeV but rises rapidly at lower energies.

In the search for cold fusion, the most detailed attention was given to the energy region of the proton peak in Fig. 1. Counts within a 120-keV interval encompassing this peak were monitored, and a wider interval of 480 keV was summed on each side of the peak to provide a simultaneous indication of background. The region of the triton peak was not used for such detailed counting because of the higher background at these energies. In order to explore the possibility of nuclear-reaction products at other energies, the entire spectrum extending to 12 MeV was visually inspected for significant peaks.

## III. SATURATION IMPLANTATION AND TEMPERATURE RAMPING

Figure 3 shows nuclear-reaction data reflecting the accumulation of D in Pd during 10-keV implantation at 41

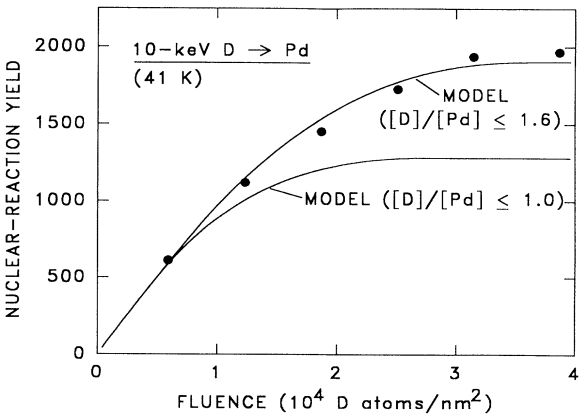


FIG. 3. Combined number of detected tritons and protons from the nuclear reaction D($d$,$p$)T during implantation of 10-keV D into Pd at 41 K. Each datum is from a 2-min interval where the incident flux was 3.6 D atoms $nm^{-2}s^{-1}$. The curves represent model calculations discussed in the text.

K. This particular specimen was in the unannealed, as-rolled condition. Each datum gives the combined number of tritons and protons detected during a 2-min interval of the implantation process while the incident flux was 3.6 D atoms $nm^{-2}s^{-1}$. An initially linear increase in nuclear-reaction yield with incident fluence is seen to give way to decreasing retention and eventual saturation. Similar series of implantations leading to saturation were carried out for the two vacuum-annealed Pd foils; one of these specimens was treated at a temperature of 41 K and the other at 81 K. The results closely reproduced the data in Fig. 3.

After implantation the above specimen was allowed to warm from 41 to 260 K; the rate varied from 2.6 K/min near 120 K to 1.6 K/min at the end. During this process the D concentration was monitored by bombarding the sample with additional D and measuring the yield from the D-D nuclear reaction. For these measurements the D energy was increased to 30 keV, thereby greatly increasing the nuclear-reaction cross section so that a smaller beam current could be used. In addition, the higher energy caused the D to be deposited at a greater depth, reducing the perturbation of the implanted region undergoing D release. Results from the temperature ramp are shown in Fig. 4. Two distinct stages of D release are apparent, one at 120 K and the other centered at about 210 K. The higher-temperature stage was previously observed in D-implanted Pd,[7] and it was successfully interpreted in terms of conventional diffusion followed by release at the surface.[8] The stage at 120 K has not been reported to our knowledge.

Quantitative interpretation of the data in Figs. 3 and 4 requires knowledge of the relationship between the concentration-versus-depth profile of the D and the number of detected nuclear-reaction products. This relationship is complicated by the fact that, as the incident deuterons continuously lose energy within the Pd matrix, there is a rapid decrease in the cross section of the reaction $D(d,p)T$. When the effects of straggling on the incident ion trajectories are neglected, one has for the yield of a particular reaction product

$$Y = N_d \Omega_d \int_{E=0}^{E_d} C_D(x(E))[\sigma(E)/4\pi][\epsilon(E,C_D)]^{-1} dE \ , \tag{1}$$

where $N_d$ is the incident number of deuterons, $\Omega_d$ is the solid angle subtended by the detector, $E_d$ is the energy of the deuteron beam, $C_D$ is the D concentration at depth $x$ expressed as D-to-Pd atomic ratio, $\sigma$ is the total nuclear cross section in the laboratory frame at instantaneous deuteron energy $E$, $\epsilon$ is the stopping power per Pd atom taking into account the presence of the D, and the energy scale is related to depth by $dE/dx = -N_h \epsilon$ with $N_h$ being the atomic density of the Pd.

The nuclear cross section in Eq. (1) is taken from the recommended formula[9]

$$\sigma(E) = [(111.0 \text{ barns keV})/E + 0.190 \text{ barns}] \times \exp[-(44.40 \text{ keV}^{1/2})/E^{1/2}] \tag{2}$$

based on measurements over the range $20 \le E \le 117$ keV. Essentially the same values were obtained in somewhat less precise experiments extending down to 6 keV.[10] The stopping power $\epsilon$ for D in Pd is equated to that for protons at the same velocity,[11] and the depth-dependent effect of lattice D on the stopping is treated as prescribed elsewhere.[12] This gives

$$\epsilon(E,C_D) = [3.70\times10^{-4} \text{ keV}^{1/2}\text{nm}^2] \times [1.0 + 0.145 C_D] E^{1/2} \ . \tag{3}$$

A second ingredient of the data analysis is information on the depth distribution and saturation behavior of the implanted D. The implantation profile for 10-keV D was calculated using the Monte Carlo range code TRIM,[13] with the result shown in Fig. 5. Also included in the figure are normalized plots of the depth-dependent cross section for the nuclear reaction $D(d,p)T$ when the imp-

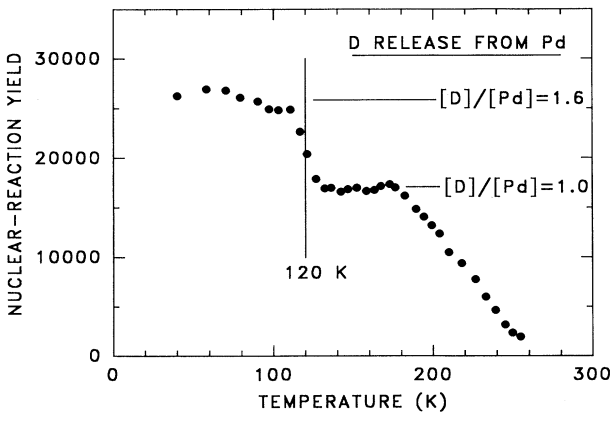


FIG. 4. Nuclear-reaction yield from D-implanted Pd during warming from 41 K. The yield was induced by bombardment with 30-keV D. The warming rate decreased from 2.6 K/min near 120 K to 1.6 K/min at the end.

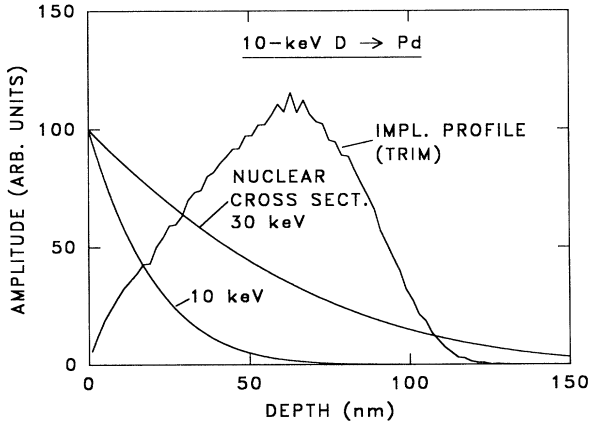


FIG. 5. Implantation profile for 10-keV D in Pd, and depth-dependent D-D nuclear cross sections for D incident onto Pd at 10 and 30 keV.

inging deuteron energy is 10 or 30 keV. These curves were calculated for zero D concentration using Eqs. (2) and (3).

Detailed depth profiles of D in Pd following high-fluence implantation at 35 K have previously been obtained using the nuclear reaction $D(^3He,\alpha)H$.[1] It was found that the D concentration at each depth increases linearly with fluence until a saturation level $C_s$ is reached, whereupon the rise in concentration abruptly stops. The published profiles show saturation in the range [D]/[Pd]=1.2–1.3, with an overall value of 1.22±0.23 being extracted. In the present analysis we incorporate the reported saturation behavior but take $C_s$ as an adjustable parameter.

The D depth profile is appreciably affected by sputtering, and this effect was included in our analysis. The reported sputtering coefficient for 10-keV D on Ag, with mass similar to Pd, is about 0.07.[14] To estimate the sputtering coefficient for the removal of PdD formula units from PdD, we multiply the Ag coefficient by the ratio of cohesion energies per formula unit for Ag and PdD. This approximation has the effect of neglecting collisions between the incident deuterons and lattice D atoms. The result is 0.07(2.96 eV)/(3.94+2.50 eV)≈0.03, where the second term in the denominator is the binding energy of D atoms in PdD.[15]

Figure 6 shows a sequence of D profiles that were calculated numerically, using the TRIM implantation profile of Fig. 5 and a formula-unit sputtering coefficient of 0.03. An appreciable fraction of the 10-keV incident D is backscattered from the specimen, and this fraction was taken to be 0.08 based on the TRIM simulation. The depth scale is referenced to the position of the Pd surface before implantation, so that the near-surface cutoff in the D profiles corresponds to the sputtered depth. In this example a saturation atomic ratio of $C_s=1.6$ was used. The nuclear-reaction yield from such D profiles is calculated by numerically performing the integration of Eq. (1).

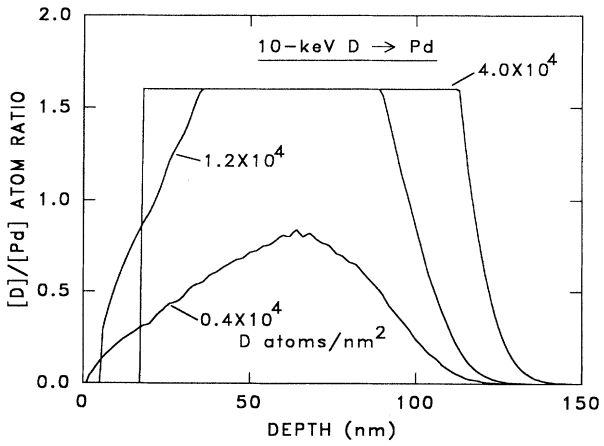


FIG. 6. Calculated depth profiles of D in Pd resulting from low-temperature implantation at 10 keV with a saturation atomic ratio [D]/[Pd] of 1.6.

The curves in Fig. 3 give the results of the above calculations as a function of implanted D fluence. Two parameters were adjusted to optimize the agreement with experiment, namely, the detector solid angle $\Omega_d$ and the saturation concentration $C_s$. The first of these quantities determines the initial slope of nuclear-reaction yield versus fluence before the onset of saturation, whereas the saturation yield at higher fluence is controlled by the product $\Omega_d C_s$. The fitted solid angle is 0.18 sr, in good agreement with the geometrically estimated value of 0.20±0.05. The extracted saturation concentration [D]/[Pd] is 1.6, with an estimated uncertainty of ±0.2. A second curve, calculated with $C_s=1.0$, is shown in Fig. 3 for comparison.

The saturation concentration obtained here is significantly greater than the value 1.22±0.23 reported in Ref. 1. This disparity is less than the combined uncertainties, however. Moreover, the apparent neglect of deuteron stopping by lattice D in the analysis of Ref. 1 would have the effect of reducing somewhat the inferred concentrations.

Consideration of Fig. 4 in the light of the above results suggests that the D-loss stage at 120 K removes the superstoichiometric condition and leaves a deuteride with composition near $Pd_1D_1$, which then undergoes release in the second stage near 210 K. The ratio of the amplitudes of the two stages is consistent with this picture, as seen in Fig. 4. The two horizontal lines show the relative decrease in nuclear-reaction yield that would be expected for a change in composition from $PdD_{1.6}$ to $PdD_{1.0}$. The ratio of the plotted heights is 1.49 rather than 1.60 because of the influence of lattice D on the deuteron stopping.

We propose that the initial stage of D loss at 120 K results from a new mechanism of accelerated D diffusion which occurs only in the concentration range $C_D>1$. Such a mechanism is qualitatively plausible on the basis of structural considerations. In particular, since there is only one octahedral interstitial solution site per metal atom in fcc Pd, lattice concentrations of D above one require the occupation of higher-energy states, and this may reduce the activation energy required to reach the diffusion saddle point. Taking the activation energy associated with the conventional diffusion stage at 210 K to be 0.23 eV,[16] one finds that a reduced activation energy of about 0.13 eV is required to account for the stage at 120 K. In Sec. IV we theoretically examine mechanisms of enhanced diffusion and identify one which semiquantitatively accounts for the experimental results.

The above discussion assumes that most of the implanted D is distributed among the interstices of the fcc Pd lattice instead of being bound in lattice defects or $D_2$ bubbles. That this is so is supported by the release behavior in Fig. 4. If the specimen instead contained a mixture of fcc $PdD_{1-\delta}$ and inhomogeneously trapped D, then the loss of D would be retarded rather than accelerated relative to a normal, undefected deuteride. This would occur because the bound D would have to be detrapped into solution before diffusion from the region of detection. We also note that *in situ* transmission-electron microscopy during high-fluence ion implantation of H into Pd

at about 20 K showed neither bubbles nor a phase transition from the fcc metal lattice.[17]

An issue not resolved by the present study is the manner of D removal from the Pd matrix during implantation beyond saturation at 41 or 81 K. We speculate that lattice disruption may occur, leading to fracture or blistering. Such effects are suggested by optical microscopy of the three implanted Pd samples after warming to room temperature. The total implanted fluences for these specimens were, respectively, $3.2\times10^4$, $3.9\times10^4$, and $5.1\times10^4$ D atoms/nm$^2$. Substantial blistering was observed at the highest fluence, as is apparent from the optical micrograph of Fig. 7, whereas none was seen at the lowest fluence, and an intermediate level was found at the middle fluence. In a similar vein, previous workers used laser-light scattering to observe surface deformation *in situ* during D implantation into Pd at 38 K.[18] They began to observe deformation at approximately the fluence where the retained quantity of D saturated.

## IV. THEORY OF DEUTERIUM DIFFUSION

In this section we explore mechanisms of enhanced D diffusion which can account for the lower-temperature stage in Fig. 4. Our point of departure is the idea that the hopping of D atoms from the low-energy octahedral sites may be enhanced by repulsive interactions with neighboring D in higher-energy sites, the latter being populated only for atomic ratios [D]/[Pd] above 1. In order to develop a specific physical picture of the mechanism, we begin by analytically treating D positional energies within a rigid lattice. Then, molecular-dynamics simulations are used to test the model.

Previous molecular-dynamics simulations of hydrogen isotopes in Pd have included calculation of the diffusion coefficient at low concentrations,[19,20] examination of D-D separations in $PdD_{1.1}$ in connection with the possibility of cold fusion,[6] and evaluation of the optic vibrational spectrum at low concentration.[21] The first three of these works used empirical two-body potentials, while Ref. 21 employed a possibly more accurate embedded-atom potential. For the present purpose of comparing diffusion in $PD_{1+\delta}$ with that in $PdD_{1-\delta}$, we deem it sufficient to use relatively simple, analytic, two-body potentials. The ones chosen are very similar to those employed in Ref. 6 to describe $PdD_{1.1}$.

The Pd-D interaction used here is actually identical to that of Ref. 6, being given by

$$V_{MD}(r)=V_0[(r_0/r)^6-2(r_0/r)^3]f_c(r/r_c) \tag{4}$$

with $V_0=0.126$ eV, $r_0=a_0/\sqrt{2}$, the cutoff distance $r_c=0.86a_0$, and

$$f_c(z)=\begin{cases}1-\exp[-10(1-z)^2] & \text{for } 0\le z\le 1\\ 0 & \text{for } z>1\ .\end{cases} \tag{5}$$

The lattice constant $a_0$ is taken to be 0.408 nm, representative of $PdD_x$ near $x=1$. The Pd-Pd interaction is also the same as in Ref. 6, being a Lennard-Jones 6-12 potential with equilibrium distance $a_0/\sqrt{2}$ and a cutoff at $0.86a_0$.

The D-D potential is expressed as a screened Coulomb interaction,

$$V_{\text{D-D}}(r)=[e^2/r]\exp[-r/r_e]\ , \tag{6}$$

where $e$ is the electron charge. The associated screening length $r_e$ is equated to 0.033 nm in order to give energy profiles for two D atoms displaced along high-symmetry directions which agree with recent first-principals total-energy calculations.[22] The value is somewhat larger than in Ref. 6; there, a minimal screening length of 0.026 nm was used to determine how close deuterons might reasonably be expected to approach one another.

Properties of the above potentials are illustrated in Figs. 8 and 9. Figure 8 shows the variation in system energy for $PdD_{1-\delta}$ as a D atom is moved along the general-

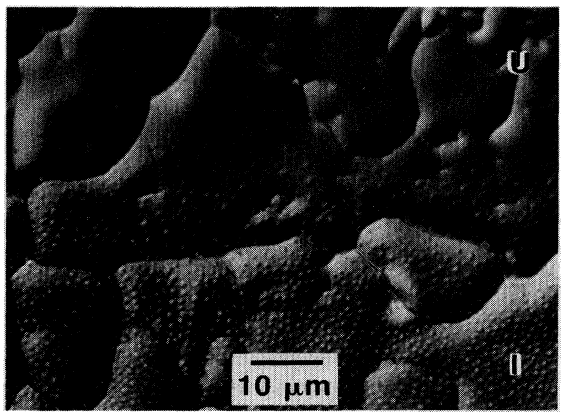


FIG. 7. Nomarski optical micrograph showing surface deformation of Pd after implantation of $5.1\times10^4$ D atoms/nm$^2$ at 10 keV and a temperature of 81 K, taken after warming to room temperature. The imagined region is at the boundary between the implanted ($I$) and unimplanted ($U$) areas. The implanted area shows numerous blisters about 1 $\mu$m in diameter.

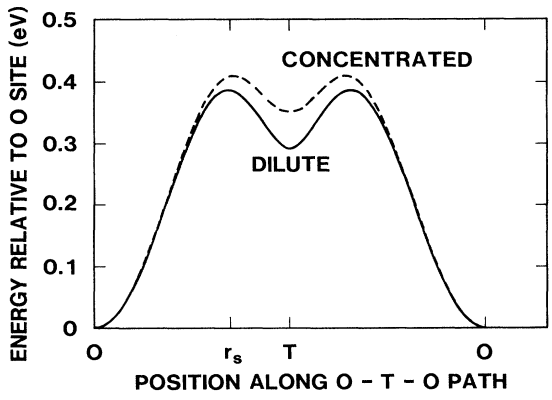


FIG. 8. Calculated energy variation for a D atom moving from one octahedral interstitial site to a second, vacant octahedral site through a tetrahedral site. The solid curve is for an isolated D atom, while the dashed curve gives the result when all neighboring octahedral sites are occupied except the target vacancy. Tetrahedral sites are unoccupied in both cases.

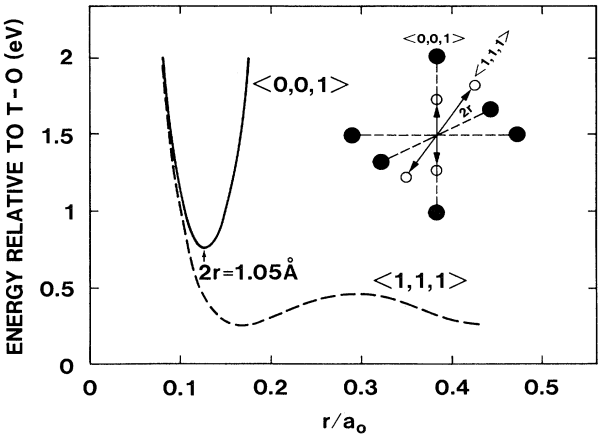


FIG. 9. Energy profiles for two D atoms symmetrically displaced from an octahedral site by distance $r$ along a [111] or [100] direction. The configuration of zero energy is defined as one D atom at an octahedral site and the other D at an adjacent tetrahedral site.

ly accepted diffusion path between octahedral solution sites. This path initially extends along a [111] direction through a saddle point to the tetrahedral interstitial site, and then along another [111] direction to the new octahedral position. Lattice relaxations are excluded in the calculation. The solid curve represents the situation with no neighboring D atoms, whereas the dashed curve shows the variation when all octahedral sites are occupied except the one to which the migrating atom moves, with the difference being due to the D-D repulsion.

Figure 9 exhibits further properties of the D-D interactions, and it directly addresses the question of whether the excess D in $PdD_{1+\delta}$ is accommodated by multiple occupancy of the octahedral sites or by partial occupation of tetrahedral interstitial sites. The plot gives the combined energy of two D atoms symmetrically positioned at distance $r$ from an octahedral center along either a [111] or [100] direction, with zero energy corresponding to one atom in an octahedral site and the other in an adjacent tetrahedral site. All of the surrounding octahedral sites are treated as occupied. The configurational energies in this figure closely reproduce those of the first-principles calculation of Ref. 22; as indicated above, the screening length in Eq. (6) was selected to produce this property. The fact that the energy is positive at all positions indicates that partial occupation of tetrahedral sites is favored over multiple occupancy of octahedral sites. It is therefore concluded that the octahedral interstitial sites in $PdD_{1+\delta}$ are singly occupied, with the excess D atoms residing in tetrahedral sites.

The above potentials will now be used to explore the mechanisms of the accelerated D diffusion that is observed in the superstoichiometric state. We hypothesize that a D atom initially occupying a low-energy octahedral site moves to a neighboring, unoccupied tetrahedral site, as also occurs at normal compositions. In $PdD_{1+\delta}$, however, this process is proposed to have a reduced activation barrier due to the correlated movement of a second D atom from a neighboring tetrahedral site into the octahedral site being vacated. The magnitude of the barrier reduction depends, of course, on the degree of correlation in the atom motions. In the extreme, uncorrelated case where an octahedral-to-tetrahedral jump is completed before the second D atom moves into the vacated site, there is no reduction. In contrast, the maximum effect is realized for an adiabatic process whereby the two atoms move so as continuously to minimize the potential energy. An intermediate, "sudden" scenario abruptly imparts kinetic energy to the tetrahedral D atom, which then moves into the octahedral position while propelling the initial occupant to the saddle point.

Figure 10 shows the potential energies associated with the above three sequences, as calculated using Eqs. (4)–(6) in a rigid Pd lattice with all octahedral sites except the target site being occupied. The curve for the "sudden" case was obtained by numerically integrating the classical equations of motion. The maximum displacement from the octahedral site is plotted as a function of energy input, with $r_s = 0.29$ nm corresponding to the diffusion saddle point. The respective activation energies for the mechanisms are 0.18, 0.29, and 0.41 eV, with the third value corresponding to conventional diffusion in $Pd_{1-\delta}$. These results indicate that the proposed crowd-atom process can indeed result in substantially accelerated diffusion.

Molecular-dynamics simulations provide a means of examining the diffusional motions of the D without the imposition of a particular hopping sequence. We performed such simulations using a host matrix of 108 Pd

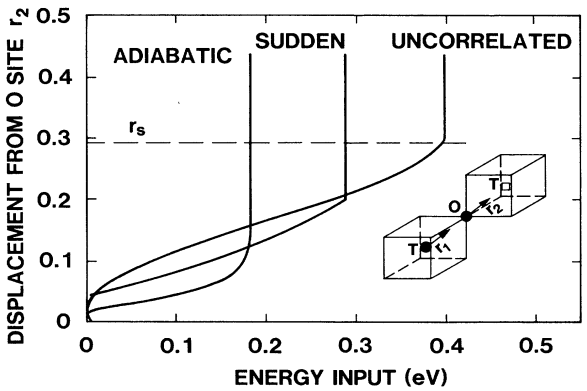


FIG. 10. Energetics for correlated diffusive motion of two D atoms initially in adjacent tetrahedral and octahedral interstitial sites. The displacement $r_2$ of the octahedral D toward an unoccupied tetrahedral site is plotted as a function of the energy input required to produce that displacement. In the uncorrelated case, the D in the tetrahedral site remains fixed as the octahedral D moves. The adiabatic process has the two atoms moving in unison so as to minimize total energy at each point. The "sudden" scenario abruptly imparts velocity to the tetrahedral D in the direction of the octahedral D, and the two atoms then move according to classical equations of motion.

atoms which contained either 97 D atoms, simulating $PdD_{0.9}$, 0r 119 D atoms, simulating $PdD_{1.1}$. Using methods discussed elsewhere,[6] calculations were carried out for temperatures from 570 to 1000 K. The temperatures of direct interest below 200 K were inaccessible to simulation because of the excessive computation time which was required. The run times were in all cases sufficient to produce rms displacements of 0.3 nm or more, and at 1000 K the displacements extended to 1 nm. The diffusion coefficient of the D was estimated on the basis of the relation

$$D_D = \lim_{t\to\infty} (\langle r^2 \rangle / 6t) , \quad (7)$$

where $\langle r^2 \rangle$ is the rms displacement and $t$ the simulation time. Plots of $\langle r^2 \rangle$ versus $t$ were made, and straight-line fits then yielded $D_D$ and its uncertainty.

Results of the simulations are shown in Fig. 11. A substantial decrease in activation energy is apparent on going from $PdD_{1-\delta}$ to $PdD_{1+\delta}$, in accord with the ideas developed above. The lines through the simulation data have slopes corresponding to activation energies of 0.41 and 0.29 eV, respectively. The first value is that from Fig. 10 for the case of uncorrelated motion, which also corresponds to conventional diffusion in $Pd_{1-\delta}$, while the second value is for the "sudden" model in Fig. 10. The close agreement of the "sudden" model with the simulations indicates that this crowd-atom diffusion mechanism is probably the correct one.

The two-body potentials used in the present calculations yield diffusion activation energies that are larger than observed experimentally: at D concentrations below $C_D = 1$, the experimental value is approximately 0.23 eV,[16] whereas the calculated value is 0.41 eV. The predicted drop in activation energy above $C_D = 1$, however, is close to that inferred in Sec. III to account for the separation of the stages at 120 and 210 K: the theoretical shift is 0.12 eV while the experimentally inferred one is 0.10 eV. While the interatomic potentials could be manipulated to produce more precise agreement with the data for diffusion at high temperatures and low concentration, such adjustments should not change the qualitative nature of the mechanism leading to the enhanced diffusion above stoichiometry.

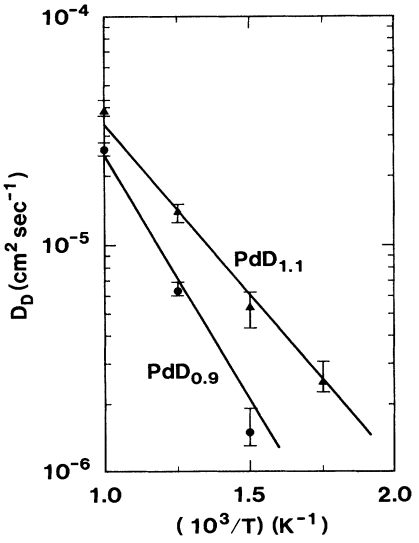


FIG. 11. Diffusion coefficient for D in $PdD_{0.9}$ and $PdD_{1.1}$ from molecular-dynamics simulations. The lines through the simulation data have slopes corresponding, respectively, to activation energies of 0.41 eV, taken from the uncorrelated mechanism in Fig. 10, and 0.29 eV from the sudden mechanism.

## V. SEARCH FOR COLD FUSION

In order to observe charged particles from possible D-D nuclear reactions within the Pd, the particle-detection system was kept active after the implantation beam was removed. Two Pd samples, one annealed and the other in the as-rolled condition, were implanted to saturation at 41 K and then held at that temperature for 1.3 and 7.0 h, respectively. A second annealed specimen was implanted to saturation at 81 K, held for 5.4 h at that temperature, and then warmed to 230 K over a period of 1.5 h while being monitored. As described in Sec. II, the detection system was configured to sense particles with energies up to 12 MeV after passage through the 2.5-$\mu$m Ni foil. We monitored the accumulation of counts in the energy interval corresponding to protons from the reaction $D(d,p)T$, and also visually inspected the full energy spectrum for the appearance of other reaction peaks. As will now be discussed, we perceive no evidence of cold fusion in these results.

Figure 12 shows a representative energy spectrum accumulated after saturation implantation of D into Pd. In this particular case the implantation was carried out at a temperature of 41 K, and the plotted data were obtained over 7 h while the sample was held at 41 K. The spectrum is very similar in shape and amplitude to the background data shown in Fig. 2, particularly when scaled to the same accumulation time. Hence there appears to be no significant evidence of charged particles from nuclear reactions within the Pd deuteride.

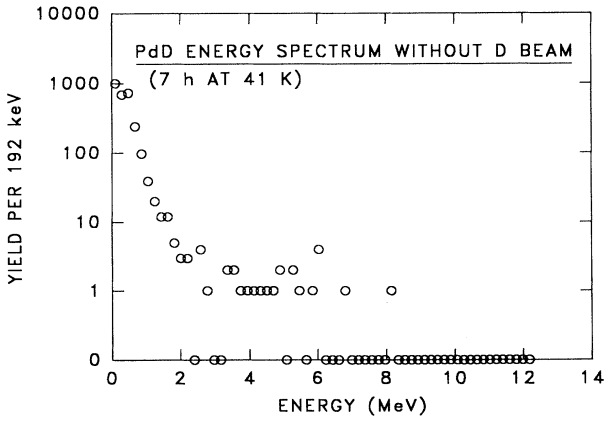


FIG. 12. Energy spectrum accumulated during 7 h while implanted PdD was held at a temperature of 41 K.

TABLE I. Results of search for energetic protons from cold fusion in D-implanted Pd.

| Foil | Temp. (K) | Time (h) | Retained D (No. atoms) | Proton counts | (Background) | Reaction rate (events/s D atom) |
|---|---|---|---|---|---|---|
| 2Pd[a] | 41 | 8.3 | $0.9\times10^{18}$ | 1 | (1.4) | $\lesssim2\times10^{-21}$ |
| Pd[b] | 81 | 5.4 | $0.9\times10^{18}$ | 0 | (0.5) | $\lesssim4\times10^{-21}$ |
| Pd[b] | 81–230 | 1.5 | $\sim0.9\times10^{18}$ | 0 | (0.3) | $\lesssim1\times10^{-20}$ |

[a]One sample annealed at 1273 K, the other unannealed.
[b]Annealed at 1273 K.

The numbers of counts within the region of the proton peak are summarized in Table I, along with estimates of the background yield based on counts in adjacent regions of the spectrum. The total number of D atoms retained within the sample is estimated by integration of the calculated concentration profile discussed in Sec. III. This number is then used to obtain the reaction-rate bounds given in the last column, taking account of the fact that only the fraction $\Omega_d/4\pi=0.016$ of emitted particles would enter the detector. Taken together, these results indicate that the fusion reaction rate in the superstoichiometric Pd deuteride is less than about $10^{-21}$ events/s D atom.

It may be noted that the above upper bound is less restrictive than those obtained in bulk Pd deuterides, where limits as small as $10^{-25}$ events/s D atom have been reported. (See, for example, Refs. 23 and 24.) The difference results primarily from the much smaller number of D atoms within the implanted layer, whose thickness is only about 100 nm. The significance of the present results is that they place a limit on fusion reactions occurring at a higher local density of deuterons, about 1.6 per metal atom compared to 1.0 or less for other reported studies.

## VI. SUMMARY

We used D-ion implantation at temperatures below 100 K to produce Pd deuteride with $[D]/[Pd]=1.6\pm0.2$, and we obtained evidence that the fcc Pd matrix is indeed highly supersaturated. The superstoichiometric state exhibited accelerated D transport leading to decay of the high concentration at temperatures near 120 K. The associated diffusion process was theoretically examined by analytical modeling and molecular-dynamics simulations, and it was shown to be consistent with a crowd-atom mechanism whereby a D atom initially in a tetrahedral interstitial site displaces a second deuteron initially in a lower-energy, octahedral site. There was no evidence of energetic charged particles from cold-fusion reactions within the superstoichiometric Pd deuteride.

## ACKNOWLEDGMENTS

The authors are indebted to D. K. Brice for useful discussions, to D. L. Overmyer for construction of the cryogenic specimen chamber, and to D. M. Bishop for assembly and calibration of the particle-detection system. This work was supported by the U.S. Department of Energy under Contract No. DE-AC04-76DP00789.

[1]W. Möller, F. Besenbacher, and J. Bøttiger, Appl. Phys. A **27**, 19 (1982).
[2]B. Baranowski, in *Hydrogen in Metals,* edited by G. Alefeld and J. Völkl (Springer-Verlag, Berlin, 1978), Vol. II, p. 168.
[3]M. Fleischmann and S. Pons, J. Electroanal. Chem. **261**, 301 (1989).
[4]S. E. Jones, E. P. Palmer, J. B. Czirr, D. L. Decker, G. L. Jensen, J. M. Thorne, S. F. Taylor, and J. Rafelski, Nature **338**, 737 (1989).
[5]S. M. Myers, D. M. Follstaedt, J. E. Schirber, and P. M. Richards, J. Fusion Energy **9**, 263 (1990).
[6]P. M. Richards, Phys. Rev. B **40**, 7966 (1989).
[7]W. Möller, Nucl. Instrum. Methods **209&210**, 773 (1983).
[8]S. M. Myers, P. M. Richards, W. R. Wampler, and F. Besenbacher, J. Nucl. Mater. **165**, 9 (1989).
[9]R. E. Brown and N. Jarmie, Phys. Rev. C **41**, 1391 (1990).
[10]A. Krauss, H. W. Becker, H. P. Trautvetter, C. Rolfs, and K. Brand, Nucl. Phys. A **465**, 150 (1987).
[11]H. H. Andersen and J. F. Ziegler, *Hydrogen Stopping Powers and Ranges in All Elements* (Pergamon, New York, 1977).
[12]D. J. Malbrough, D. K. Brice, D. F. Cowgill, J. A. Borders, L. A. Shope, and J. M. Harris, Nucl. Instrum. Methods B **28**, 459 (1987).
[13]J. F. Ziegler, J. P. Biersack, and U. Littmark, *The Stopping and Range of Ions in Solids* (Pergamon, New York, 1985).
[14]H. H. Andersen and H. L. Bay, in *Sputtering by Particle Bombardment,* edited by R. Behrisch (Springer-Verlag, Berlin, 1981), Vol. I, p. 182.
[15]E. Wicke and H. Brodowsky, in *Hydrogen in Metals,* edited by G. Alefeld and J. Völkl (Springer-Verlag, Berlin, 1978), Vol. II, p. 82.
[16]J. Völkl and G. Alefeld, in *Hydrogen in Metals,* edited by G. Alefeld and J. Völkl (Springer-Verlag, Berlin, 1978), Vol. I, p. 325.
[17]X. W. Lin. M. O. Ruault, A. Traverse, J. Chaumont, M. Salomé, and H. Bernas, Phys. Rev. Lett. **56**, 1835 (1986).
[18]W. Möller, F. Besenbacher, and T. Laursen, J. Nucl. Mater. **93&94**, 750 (1980).
[19]M. J. Gillan, J. Phys. C **19**, 6169 (1986).
[20]J. W. Culvahouse and P. M. Richards, Phys. Rev. B **38**, 10020 (1988).
[21]L. R. Pratt and J. Eckert, Phys. Rev. B **39**, 13170 (1989).
[22]X. W. Wang, S. G. Louie, and M. L. Cohen, Phys. Rev. B **40**, 5822 (1989).
[23]J. E. Schirber, M. A. Butler, D. S. Ginley, and R. I. Ewing, Fusion Technol. **16**, 397 (1989).
[24]J. F. Ziegler, T. H. Zabel, J. J. Cuomo, V. A. Brusic, G. S. Cargill III, J. O'Sullivan, and A. D. Marwick, Phys. Rev. Lett. **62**, 2929 (1989).

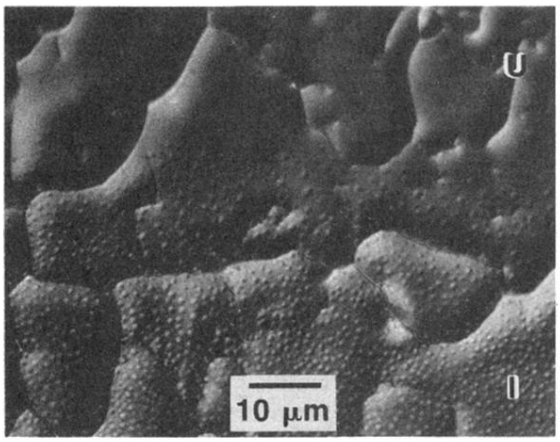


FIG. 7. Nomarski optical micrograph showing surface deformation of Pd after implantation of $5.1 \times 10^4$ D atoms/nm$^2$ at 10 keV and a temperature of 81 K, taken after warming to room temperature. The imagined region is at the boundary between the implanted ($I$) and unimplanted ($U$) areas. The implanted area shows numerous blisters about 1 $\mu$m in diameter.